Study on Shear Rate Effects in Direct Shear Tests at Saturated Soil–Geotextile Interfaces

Jianhua Dong, Jianhua Huang*, Pengfei He

Lanzhou University of Technology, Lanzhou City, China

*2584849660@qq.com

Abstract. The shear rate effect on saturated soil–geotextile interface behavior was investigated through modified direct shear tests on silty clay from the Lanzhou New District, China, under four normal stress levels (25–100 kPa) and four shear rates (0.02–1.2 mm/min). Results show that all shear stress–displacement curves exhibited strain-hardening behavior without post-peak softening, with ultimate shear stress increasing approximately linearly with normal stress. A pronounced negative rate dependence was identified: at 50 kPa normal stress, steady-state shear strength decreased from 45 kPa to 36 kPa (20% reduction) as shear rate increased from 0.02 to 1.2 mm/min. Contractive deformation increased with normal stress but decreased with shear rate, declining from 0.6 mm to 0.3 mm over the tested range. The underlying mechanism is attributed to a gradual drainage transition: low shear rates maintained near-drained conditions with limited excess pore pressure (5–7 kPa), whereas high rates induced significant pore pressure accumulation (18 kPa), reducing effective stress and suppressing both strength mobilization and contractive deformation. These findings inform interface parameter selection for geosynthetic-reinforced structures in seasonally frozen regions.

Keywords: saturated soil–geotextile interface; direct shear test; shear rate effect; negative rate dependence; excess pore water pressure; contractive deformation

1 Introduction

With the rapid advancement of modern geotechnical engineering, geotextiles—as a category of novel engineering materials—have been extensively employed in a wide range of applications, including slope stabilization, ground improvement, earth retaining structures, and landfill closure cover systems(e.g.1). The adoption of these geosynthetic materials has provided more cost-effective and environmentally sustainable alternatives to conventional geotechnical solutions(e.g.2) . Geotextiles are primarily manufactured from high-molecular-weight polymers, engineering plastics, and synthetic fibers, and function through embedment within the soil mass, surface coverage, or interlayer placement to achieve soil reinforcement and protection. In seepage control applications, geomembranes play an essential role in municipal solid waste dis-

J. Zhang et al. (eds.), *Proceedings of the 2026 2nd International Conference on Engineering Management and Safety Engineering (EMSE 2026)*, Advances in Engineering Research 300,
https://doi.org/10.2991/978-94-6239-703-3_17

posal facilities, wastewater treatment systems, artificial water bodies, and aquaculture installations(Fig.1).Meanwhile, specialty geotextiles and their composite products are frequently utilized to construct multi-layer impervious barrier systems or to serve multiple functions such as separation, filtration, drainage, and structural protection.

Fig. 1. The Application of Geotextiles in Engineering

It is well established that the shear strength behavior of soils is influenced by the shear rate. Extensive experimental investigations have been conducted by researchers both domestically and internationally at the levels of the soil element and the reinforcement–soil interface, yielding a substantial body of knowledge on this topic(e.g.3).

Regarding the influence of shear rate on soil strength, existing studies have revealed significant differences in rate sensitivity among various soil types, along with their underlying mechanisms. For normally consolidated cohesive soils, shear strength generally increases with increasing strain rate(e.g.4), with the internal friction angle exhibiting a monotonically increasing trend and cohesion displaying an inverse relationship(e.g.5). Under overconsolidated conditions, higher overconsolidation ratios are typically associated with lower excess pore water pressures, while increasing shear rates lead to enhanced undrained shear strength and reduced excess pore water pressures(e.g.6). For reconstituted saturated cohesive soils, the effects of shear rate on shear displacement–stress curves and shear strength under both normally consolidated and overconsolidated conditions have been systematically elucidated(e.g.7). Investigations of soft clays using integrated true triaxial and nuclear magnetic resonance testing have demonstrated that load level and shear strain rate jointly govern the mechanical response characteristics and microstructural evolution of soft clays(e.g.8). However, the manifestation of rate effects differs markedly for gravelly and sandy soils: the peak stress of gravelly soils decreases significantly with increasing strain rate(e.g.9); the shear strength of sand under high-stress conditions is subject to the coupled influence of normal stress and shear rate, which modulate macroscopic strength through mesoscale mechanisms such as particle crushing and rearrangement(e.g.10). For saturated loess, confining pressure and shear rate exert significant interactive effects on stress–strain behavior and shear strength(e.g.11).

Drainage conditions constitute a key factor modulating shear rate effects. Systematic studies have demonstrated that the shear strength of saturated sand decreases with increasing shear rate under drained conditions, whereas no significant variation has

been observed under undrained conditions(e.g.12), with the strength under drained conditions being generally higher than that under undrained conditions(e.g.13). This phenomenon can be interpreted from the perspective of excess pore water pressure generation and dissipation: as the shear rate increases, soil behavior transitions sequentially through fully drained (no pore pressure accumulation), partially drained (partial pore pressure accumulation), and fully undrained (complete pore pressure retention) stages, with viscous rate effects superimposed(e.g.14). This gradual transition from drained to undrained conditions provides a unified framework for understanding rate-dependent effects.

At the level of the reinforcement–soil and structure–soil interfaces, significant progress has also been achieved in understanding rate effects. The variation of interface characteristics with shear rate follows patterns analogous to those observed in bulk soil, adhering to the fundamental paradigm of gradual drainage state transition . Studies employing modified triaxial tests and simple direct shear tests have demonstrated that shear rate is directly related to interface strength softening mechanisms, with interface dilatancy behavior being significantly influenced by interface pore pressure(e.g.15), and coupled effects of interface roughness and shear rate on deviatoric stress, excess pore pressure, and stress paths have been documented. In the domain of reinforced soil interfaces, direct shear and pullout tests have confirmed that shear rate and reinforcement properties (e.g., differences between geogrids and geotextiles) jointly influence the mobilization of reinforcement–soil interface strength . Furthermore, the observed increase in pile shaft shearing resistance at high penetration rates corroborates the significant role of viscous effects in interface mechanical behavior, which are closely associated with pore water, inter-particle contacts, and soil–skeleton interactions(e.g.16).

In summary, although existing research has produced abundant results on shear rate effects in bulk soils and at structure–soil interfaces, systematic investigations of the strength characteristics, deformation behavior, and pore water pressure response mechanisms at the saturated soil–geotextile interface under varying shear rates remain comparatively scarce. There is a pressing need to elucidate these mechanisms through dedicated direct shear testing programs.

2 Materials and Methods

2.1 Physical Properties of the Test Soil

The soil used in this experimental program was sampled from the Lanzhou New District, Gansu Province, China, which is located within a seasonally frozen region. Samples were retrieved from a depth of approximately 1 m. In accordance with the soil classification standard,the material was classified as silty clay. The physical and mechanical properties of the test soil are of critical importance to interface behavior and were therefore comprehensively characterized, including natural water content, saturated water content, optimum water content, particle size distribution, liquid and plastic limits, internal friction angle, cohesion, and maximum dry density. These in-

dex properties are summarized in Table 1. The grain size distribution curve of the soil is depicted in Fig.2.

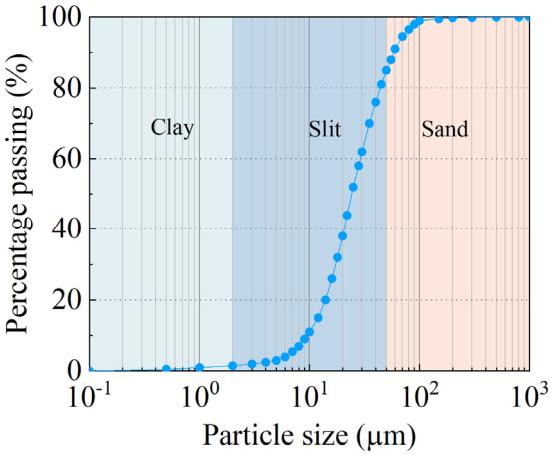

Fig. 2. Grain Size Distribution Curve

Table 1. Basic physical and mechanical properties of soil

Soil classification	Plastic limit(%)	Liquid limit(%)	Maximum drydensity (g/cm³)	IP
Silty clay	13.8	29.1	1.02	15.3

2.2 Specimen Preparation

Air-dried soil samples were first disaggregated using a rubber mallet and passed through a 2 mm standard sieve. The sieved material was subsequently placed in an oven maintained at 105°C and dried to constant mass (no less than 24 h), then cooled to ambient temperature and sealed in a desiccator for storage. Based on the maximum dry density and a target degree of compaction, the required mass of dry soil was calculated for the specimen dimensions of 100 mm × 100 mm × 35 mm. The dry soil was thoroughly mixed with distilled water to achieve the target water content, sealed in polyethylene bags, and cured for 48 h to ensure uniform moisture distribution.

Prior to specimen preparation, the geotextile was trimmed to dimensions slightly exceeding those of the acrylic plate and uniformly bonded to the rigid block (100 mm × 100 mm × 10 mm) using high-strength adhesive, ensuring a flat and wrinkle-free surface. A rigid plate was placed on top and uniform pressure was applied for 24 h to guarantee adequate bonding between the geotextile and the acrylic substrate, thereby preventing debonding or relative slippage during shearing. Following curing, the acrylic plate with the bonded geotextile was placed at the bottom of the specimen mold (geotextile side facing upward), and the cured soil was compacted into specimens of 100 mm × 100 mm × 35 mm by layered tamping, with scarification between successive layers to ensure satisfactory interlayer bonding. After demolding, each

specimen was carefully wrapped and secured with filter paper to prevent particle loss, then placed in layers within a vacuum chamber.

Following specimen preparation, samples requiring saturation were carefully wrapped in filter paper, systematically placed in the vacuum chamber with adequate spacing between layers to facilitate uniform water infiltration, and the chamber lid was sealed with petroleum jelly applied along the joint to prevent air leakage during evacuation. The vacuum pump was connected to the chamber via tubing and activated; the chamber pressure was reduced to approximately −100 kPa within 10 min, after which the vacuum state was maintained for at least 0.5 h to ensure thorough removal of entrapped air from micropores within the specimens. The vacuum pump was then deactivated, seal integrity of all valves and connections was verified, and the water inlet valve was slowly opened at a controlled rate to avoid hydraulic disturbance to the specimen structure. The specimens were immersed for no less than 10 h under stable water level conditions without any movement or contact, allowing complete displacement of entrapped air from specimen pores to achieve full saturation.

2.3 Experimental Apparatus

The direct shear tests were conducted using a TKA-DDS-5A microprocessor-controlled direct shear apparatus. The instrument is equipped with an integrated microprocessor and a human-machine interface control panel, enabling automated shear box positioning, as well as simultaneous acquisition of horizontal load and displacement data. The shear box has internal dimensions of 100 mm × 100 mm × 50 mm, with both the upper and lower halves having a height of 25 mm. The apparatus has a maximum shear displacement capacity of 12 mm and a maximum horizontal shear force of 10 kN.

2.4 Pore Water Pressure Measurement

The pore water pressure at the interface was measured using the method proposed by Sharma (e.g.17). In this approach, a 5 mm diameter hole was drilled through the loading plate of the direct shear box, positioned as close to the center as possible, to accommodate a miniature pore water pressure transducer. After the soil was compacted to the required density, a 6 mm diameter borehole was drilled from the specimen surface to a depth of 23 mm using a hand auger. The miniature pore water pressure transducer was then inserted into the borehole, which was subsequently backfilled with the same soil and recompacted.

3 Results

3.1 Shear Stress-Displacement Curves

Fig.3 presents the shear stress–displacement curves of the saturated soil–geotextile interface under constant normal stress (σ = 50 kPa) at various shear rates (v = 0.02,

0.1, 0.8, and 1.2 mm/min). All test conditions exhibited strain-hardening responses with no apparent post-peak softening. The results revealed a significant negative rate-dependent effect: as the shear rate increased from 0.02 to 1.2 mm/min, the steady-state shear strength decreased from approximately 45 kPa to 36 kPa, representing a reduction of about 20%. This phenomenon can be mechanistically explained by the pore water pressure response shown in Fig.4. Under the lowest shear rate (0.02 mm/min), the excess pore water pressure remained consistently low (approximately 5–7 kPa), indicating a nearly drained condition at the interface. With increasing shear rate, pore pressure accumulation became significantly more pronounced, reaching a peak value of approximately 18 kPa at v = 1.2 mm/min — an increase of over 200% compared to the quasi-static condition. At higher rates, the pore pressure curves exhibited a characteristic rise-then-decline pattern, with the peak occurring at a horizontal displacement of approximately 4–5 mm, corresponding to the full mobilization of the interface shear band and subsequent structural reorganization.

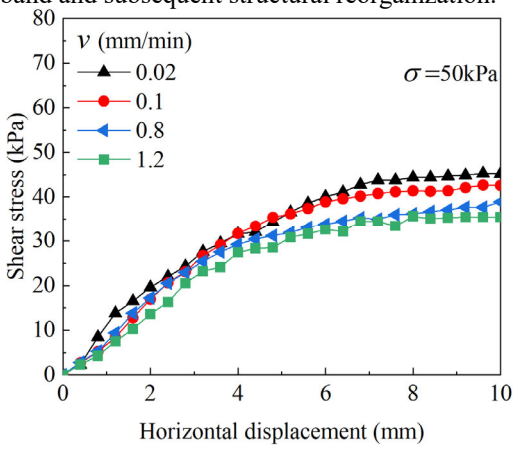

Fig. 3. Shear stress–shear displacement curves at different shear rates

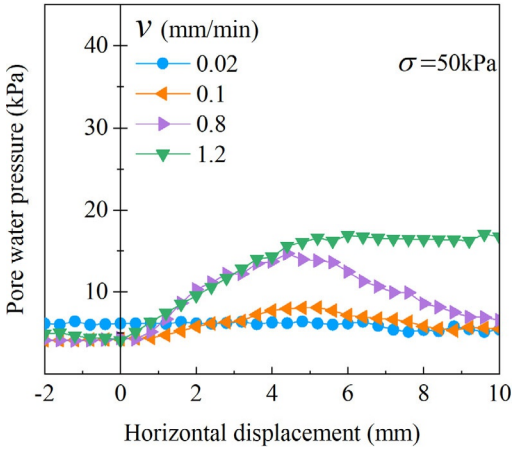

Fig. 4. Pore Water Pressure Evolution Curve

3.2 Normal Displacement Curve

Figure 5 illustrates the inverse relationship between vertical displacement and shear rate under identical test conditions: the ultimate contraction reached 0.6 mm at the low rate (0.02 mm/min) but was reduced to only 0.3 mm at the high rate (1.2 mm/min), a decrease of approximately 50%, exhibiting a pronounced suppression effect. This phenomenon can be explained through the dual mechanisms of effective stress and drainage conditions. During low-rate shearing, the ample shearing duration permits sufficient time for pore water to dissipate from the shear band to surrounding regions, maintaining the interface in a near-drained state where the effective normal stress closely approximates the applied total normal stress. The sustained high effective stress acting on the soil skeleton facilitates thorough particle sliding, rearrangement, and progressive densification within the shear band, with inter-particle voids progressively compressed and closed, manifesting macroscopically as substantial contractive deformation. Under high-rate shearing conditions, pore water within the shear band cannot dissipate in a timely manner, resulting in significant excess pore water pressure accumulation that partially sustains the externally applied normal load, thereby markedly reducing the effective stress acting on the soil skeleton. The reduction in effective stress diminishes inter-particle contact forces on one hand, weakening the driving force for relative particle sliding against interlocking and frictional resistance; on the other hand, the elevated pore water pressure impedes particle reorientation and densification. The combined action of these two factors ultimately constrains the full development of contractive volumetric response, resulting in significantly lower contraction under high-rate conditions compared to low-rate conditions.

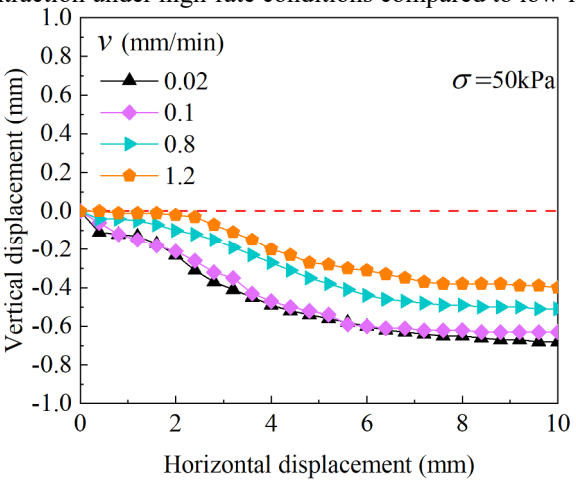

Fig. 5. Shear displacement–vertical displacement relationship curves under different shear rates

Table 2 summarizes the peak shear stress, peak pore water pressure, and peak normal displacement measured under normal stresses of 25, 50, 75, and 100 kPa at shear rates ranging from 0.02 to 1.2 mm/min. Under all normal stress levels, an increase in shear rate resulted in a progressive reduction in peak shear stress, accompanied by a

corresponding rise in peak pore water pressure and less pronounced normal contraction. For instance, at a normal stress of 100 kPa, the peak shear stress decreased from 82.0 kPa at 0.02 mm/min to 66.7 kPa at 1.2 mm/min, representing an approximate reduction of 18.7%, while the peak pore water pressure increased from 14.4 kPa to 30.7 kPa over the same rate range. This rate-dependent behavior can be attributed to the limited dissipation of excess pore water pressure at higher shear rates, which reduces the effective normal stress acting on the shear plane and consequently lowers the mobilized shear resistance. Furthermore, the magnitude of rate-induced strength degradation became more significant under higher normal stresses, suggesting a coupled effect between normal stress level and shear rate on the undrained shear response of the tested material.

Table 2. Effects of shear rate on peak shear stress, pore water pressure, and normal displacement under different normal stresses

Normal stress (kPa)	Shear rate (mm/min)	Peak shear stress (kPa)	Peak pore water pressure (kPa)	Peak normal displacement (mm)
25	0.02	25.1	2.7	-0.58
	0.1	22.3	4.4	-0.55
	0.8	21.8	8.3	-0.46
	1.2	19.9	10.5	-0.37
50	0.02	44.4	6.4	-0.65
	0.1	41.4	7.7	-0.62
	0.8	37.7	13.7	-0.49
	1.2	35.1	16.5	-0.38
75	0.02	70.8	10.7	-0.68
	0.1	66.6	15.1	-0.64
	0.8	60.1	19.1	-0.57
	1.2	50.3	21.2	-0.46
100	0.02	82	14.4	-0.79
	0.1	80.8	20.9	-0.72
	0.8	72.3	25.9	-0.66
	1.2	66.7	30.7	-0.53

4 Conclusion

This study systematically investigated the shear mechanical behavior, deformation characteristics, and pore water pressure response mechanisms of the saturated soil–geotextile interface under varying normal stress levels (25–100 kPa) and shear rates (0.02–1.2 mm/min) through direct shear testing. The principal conclusions are as follows:

(1) Under all tested conditions, the saturated soil–geotextile interface exhibited strain-hardening shear response, with shear stress increasing monotonically with horizontal displacement and gradually approaching a stable residual value, with no post-peak softening behavior observed. The ultimate shear stress increased approximately linearly with increasing normal stress, attributable to the deeper embedment of soil

particles into the geotextile fiber interstices under elevated normal stresses, which enhanced micro-scale mechanical interlocking and frictional coupling at the interface.

(2) The saturated soil–geotextile interface exhibited a pronounced negative rate-dependent effect. Under a constant normal stress of 50 kPa, the steady-state shear strength decreased from approximately 45 kPa to 36 kPa (a reduction of approximately 20%) as the shear rate increased from 0.02 mm/min to 1.2 mm/min. The underlying mechanism of this negative rate effect lies in the fact that, under high shear rate conditions, pore water cannot dissipate in a timely manner, resulting in significant excess pore water pressure accumulation (increasing from 5–7 kPa under quasi-static conditions to approximately 18 kPa at 1.2 mm/min), which reduces effective stress, weakens interface frictional resistance, and consequently diminishes the mobilization of interface shear strength.

(3) The fundamental nature of the shear rate effect can be attributed to the gradual transition in drainage conditions. At low shear rates, the interface operates under a near-drained regime with complete pore water dissipation, effective stress closely approximating total stress, and thorough development of inter-particle frictional interlocking and rearrangement. With increasing shear rate, the interface transitions progressively from a drained state through partially drained to an undrained state. The sustained accumulation of excess pore water pressure diminishes the effective stress level while simultaneously impeding particle reorientation and densification, ultimately resulting in the macroscopic mechanical responses of reduced interface strength and diminished contractive deformation.

References

1. Koerner R M. Designing with geosynthetics-Vol. 1 [M]. Xlibris Corporation, 2012.
2. Holtz R D. 46th Terzaghi lecture: geosynthetic reinforced soil: from the experimental to the familiar [J]. Journal of Geotechnical and Geoenvironmental Engineering, 2017, 143(9): 03117001.
3. Zhao Y, Li X, Liu L. Measurement of unsaturated soil shear strength through drained-vented triaxial tests[J]. Journal of Rock Mechanics and Geotechnical Engineering, 2025.
4. Ads A, Dinotte J, Omidvar M, et al. Influence of high-strain rate on the shear strength of normally consolidated kaolin clay[J]. Acta Geotechnica, 2025, 20(8): 4183-4197.
5. Zhang H Y, Hu X L, Liu X Y, et al. Effects of water content and shear rate on the shear behavior and damage evolution of cohesive slip zone soil [J]. Rock and Soil Mechanics, 2025, 46(08): 2471–2482.
6. Wu S, Lok T, Xu Y, et al. Rate-dependent behavior of a saturated reconstituted clay under different over-consolidation ratios and sample variance [J]. Acta Geotechnica, 2021, 16(11): 3425–3438.
7. Shi B T. Experimental study on the effect of direct shear test shear rate on the strength of cohesive soils [D]. Nanjing University, 2014.
8. Jiang Y, Xu Z, Liu R. An Incorporating Pore Water Pressure Constitutive Model for Over-consolidated Clay and Calibration of Transient FE Parameters[J]. Journal of Marine Science and Engineering, 2026, 14(4): 376.

9. Sheng Y, Liao X, Liu Y, et al. The effect of particle characteristics on the frictional behavior of gravel exposed to dynamic normal stress[J]. Soil Dynamics and Earthquake Engineering, 2025, 198: 109568.
10. Dong Z L, Tong C X, Zhang S, et al. Strength and dilatancy of crushable soils with different gradings[J] Canadian Geotechnical Journal, 2024, 62: 1-21.
11. Zhang T, Li S, Lan H, et al. Influences of strain rate on mechanical behaviors of unsaturated and quasi-saturated loess under varying drainage conditions[J]. Journal of Rock Mechanics and Geotechnical Engineering, 2025, 17(2): 1163-1181.
12. Chen J, Olson S M, Banerjee S, et al. An experimental investigation of the effect of strain rate and stress path on undrained response of nonplastic soils in direct simple shear mode[J]. Canadian Geotechnical Journal, 2024, 62: 1-18.
13. Miao H, Wang G. Shear rate effect on the residual strength of saturated clayey and granular soils under low-to high-rate continuous shearing[J]. Engineering Geology, 2022, 308: 106821.
14. Huang B, Cai S, Li J, et al. Undrained strength of clay determined from simple shear test[J]. Frontiers in Earth Science, 2023, 10: 1098846.
15. Liu S, Liao C, Su X, et al. Shear rate and roughness effect on clay-steel interface strength properties in CU and CPD drainage conditions[J]. Ocean Engineering, 2024, 305: 117956.
16. Liu S, Liao C, Chen J, et al. Shear rate effect on clay structure interface strength properties in various interface boundary conditions [J]. Soil Dynamics and Earthquake Engineering, 2024, 177: 108389.
17. Fleming I R, Sharma J S, Jogi M B. Shear strength of geomembrane–soil interface under unsaturated conditions[J]. Geotextiles and Geomembranes, 2006, 24(5): 274-284.